On the stability of the disordered molecular alloy phase of ammonia hemihydrate

On the stability of the disordered molecular alloy phase of ammonia hemihydrate

C. W. Wilson, C. L. Bull, G. W. Stinton, D. M. Amos, M.-E. Donnelly, and J. S. Loveday

Citation: The Journal of Chemical Physics **142**, 094707 (2015); doi: 10.1063/1.4913684
View online: http://dx.doi.org/10.1063/1.4913684
View Table of Contents: http://scitation.aip.org/content/aip/journal/jcp/142/9?ver=pdfcov
Published by the AIP Publishing

On the stability of the disordered molecular alloy phase of ammonia hemihydrate

C. W. Wilson,[1,2] C. L. Bull,[2,3] G. W. Stinton,[2] D. M. Amos,[2] M.-E. Donnelly,[2] and J. S. Loveday[2]
[1]*Diamond Light Source, Ltd., Harwell, Didcot, Oxfordshire OX11 0DE, United Kingdom*
[2]*SUPA, School of Physics and Astronomy, Centre for Science at Extreme Conditions, University of Edinburgh, Edinburgh EH9 3JZ, United Kingdom*
[3]*ISIS Facility, STFC Rutherford Appleton Laboratory, Harwell, Didcot, Oxfordshire OX11 0QX, United Kingdom*

(Received 6 November 2014; accepted 16 February 2015; published online 5 March 2015)

The disordered-molecular-alloy phase (DMA) of ammonia hydrates [J. S. Loveday and R. J. Nelmes, Phys. Rev. Lett. **83**, 4329 (1999)] is unique in that it has substitutional disorder of ammonia and water over the molecular sites of a body centred cubic lattice. Whilst this structure has been observed in ammonia di- and mono-hydrate compositions, it has not been conclusively observed in the ammonia hemihydrate system. This work presents investigations of the structural behaviour of ammonia hemihydrate as a function of P and T. The indications of earlier studies [Ma *et al.* RSC Adv. **2**, 4290 (2012)] that the DMA structure could be produced by compression of ammonia hemihydrate above 20 GPa at ambient temperature are confirmed. In addition, the DMA structure was found to form reversibly both from the melt, and on warming of ammonia hemihydrate phase-II, in the pressure range between 4 and 8 GPa. The route used to make the DMA structure from ammonia mono- and di-hydrates—compression at 170 K to 6 GPa followed by warming to ambient temperature—was found not to produce the DMA structure for ammonia hemihydrate. These results provide the first strong evidence that DMA is a thermodynamically stable form. A high-pressure phase diagram for ammonia hemihydrate is proposed which has importance for planetary modelling. © *2015 AIP Publishing LLC.* [http://dx.doi.org/10.1063/1.4913684]

I. INTRODUCTION

Ammonia and water are two of the most abundant molecules in the outer solar system and make up a significant fraction of the interiors of the ice giants Uranus and Neptune[1] and icy satellites such as Titan and Triton.[2] An in-depth understanding of how these molecules behave at high pressure is thus of great importance to models of the formation and internal dynamics of these planets and moons. Information on the different structural phases that form in this binary system and on how the two components speciate over the pressure and temperature (P-T) region relevant to planetary interiors (from 2-6 GPa for icy satellites[3] and up to 800 GPa for the ice giants[4]), would allow more accurate models to be constructed. Additionally, the ammonia-water system is one of the simplest systems to contain mixed (N–H $\cdots$ O and O–H $\cdots$ N) hydrogen bonds. Such bonds are widely found in biology and, for example, along with unmixed O–H $\cdots$ O bonds they are responsible for the base pairings in DNA.[5] High-pressure studies of ammonia hydrates provide information about the effect of compression on the geometry and strength of mixed H-bonds over a wide range of densities.

Ammonia and water are readily miscible and solidify into three stoichiometric forms; ammonia dihydrate (ADH, $NH_3{\cdot}2H_2O$), ammonia monohydrate (AMH, $NH_3{\cdot}H_2O$), and ammonia hemihydrate (AHH, $2NH_3{\cdot}H_2O$). During the formation of the solar system, the abundance of ammonia is thought to be ~15% of the nebula (the gas and dust that the sun and planets were formed from) in the outer solar system.[6] In contrast, the abundance of water is thought to be ~45%[7] and it is for this reason more effort has been made to investigate the structures and phase transitions on the water-rich side of the ammonia-water composition diagram and hence to focus on AMH and ADH. However, we have recently shown by x-ray and neutron diffraction studies that at 290 K 1:1 ammonia:water composition mixtures crystallise at ~3.5 GPa to form a mixture of AHH phase-II and water ice.[8] This would suggest that AHH may be more important to planetary models than had previously been thought since the conditions within the interiors of planets are well above this pressure. AHH-II has a monoclinic structure with space group $P2_1/c$ and lattice parameters a = 3.3584(5) Å, b = 9.215(1) Å, c = 8.933(1) Å, and β = 94.331(8)° at 3.5 GPa. This structure, shown in Figure 1, has full orientational order of all molecules and although weak evidence exists for substitutional disorder (water occupying ammonia sites and vice versa),[8] this substitutional disorder is small (at a level less than 10%). The molecular packing where the water and ammonia molecules form a series of crowned hexagonal hydrogen-bonded layers is similar to that found in ice VII—and also the disordered molecular alloy (DMA) structure described below.[8] However, the hydrogen bonding of AHH-II is significantly different from that of ice VII or DMA.[8]

However, the phase diagram is complicated by the fact that ammonia and water have been observed to form a molecular

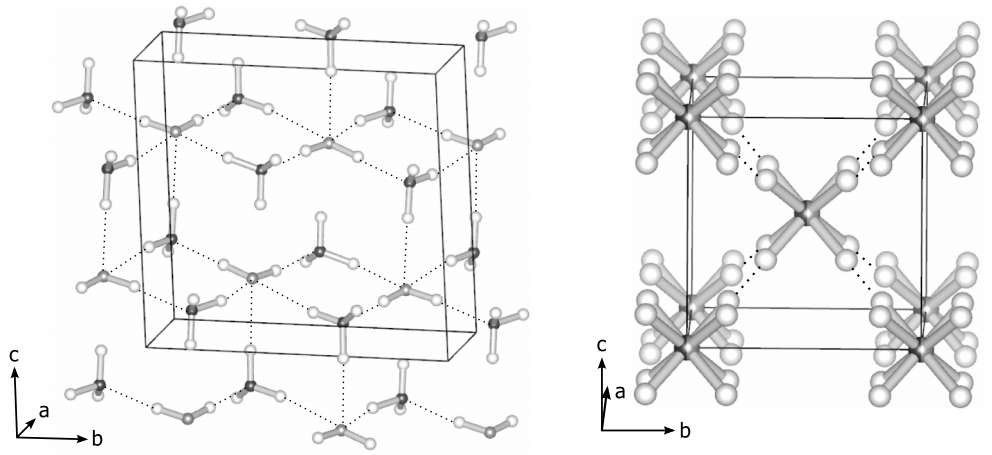

FIG. 1. The structures of AHH-II (left)[8] and DMA (right).[9] Nitrogen atoms are dark grey, oxygen atoms are light grey, hydrogen atoms are white. The light grey/dark grey atomic sites in the DMA structure show that either site can be occupied by either an oxygen or a nitrogen atom. In the DMA structure, the hydrogen sites are only partially occupied and the hydrogen sites in the ⟨110⟩ directions have been omitted for clarity. The dotted lines on both structures represent the hydrogen bonds between the molecules. Detailed descriptions of the structures can be found in Refs. 8 and 9.

alloy at high pressure.[9] This structure is unique in molecular systems in that it has full random substitutional disorder of water and ammonia on the sites of a body-centred cubic structure. It was first observed in samples of 1:1 ammonia:water composition that had been compressed to ~6 GPa and warmed to room temperature[9] and subsequently in samples of 1:2 ammonia:water composition compressed along a similar route.[10] These P-T paths are shown as dashed arrow lines on the AMH and ADH phase diagrams in Figure 2. The same cubic structure can accommodate both compositions (1:1 and 1:2) because of the substitutional disorder and the two forms differ simply in the probability of a given bcc site being occupied by a water or an ammonia molecule. The DMA structure is cubic with space group $Im\bar{3}m$ and has a lattice parameter a = 3.2727(2) Å for a 1:1 composition at 5.5 GPa[9] and 3.3141(6) Å for a 1:2 composition at 5.5-6 GPa.[10] Figure 1 shows the DMA structure along with the AHH-II structure for comparison. It has been suggested that, because of this substitutional disorder, the DMA structure could accommodate a wide range of non-stoichiometric hydrate compositions and thus be the ultimate high-pressure form of a wide range of hydrate compositions.[9] However, the situation remains unclear since both 1:1 and 1:2 compositions when compressed at room temperature solidify to form mixtures of AHH-II and ice VII.[8] Recent x-ray diffraction, Raman and infra-red spectroscopic studies by Ma *et al.* also explored the behaviour of a 2:1 composition up to ~40 GPa.[11] They concluded that the sample crystallised to an orthorhombic structure at 3.5 GPa which subsequently transformed to DMA at 19 GPa and then underwent a further transition at 25 GPa where a new reflection appears at ~1.875 Å. These conclusions are somewhat surprising. They disagree with our conclusions—based

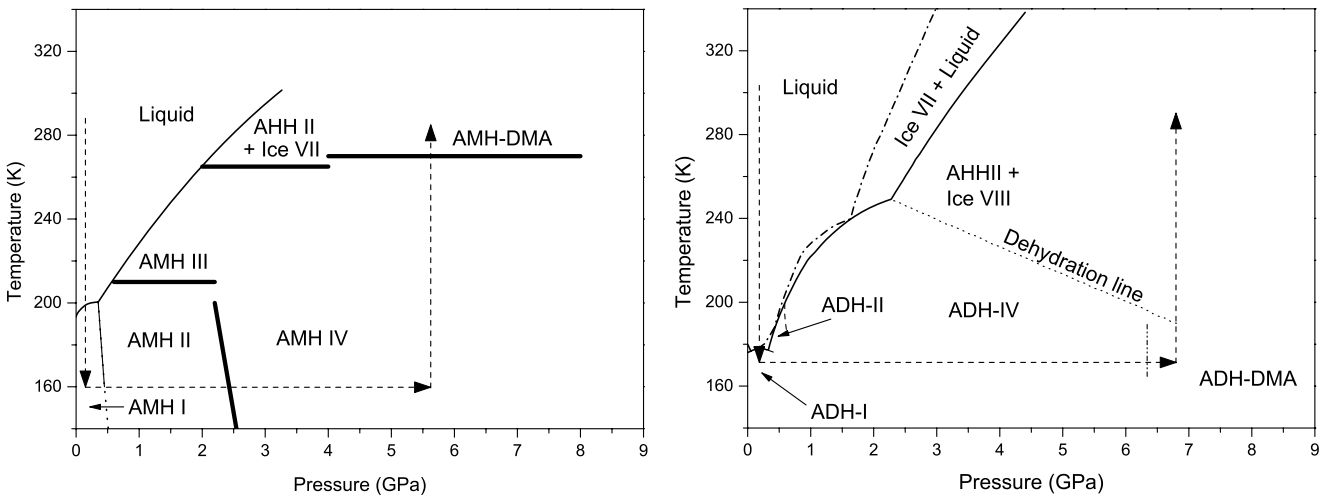

FIG. 2. The phase diagrams of both AMH (left)[14] and ADH (right),[24] respectively. The thick black lines on the AMH phase diagram show the approximate positions of phase transition lines. The dotted-dashed line on the ADH phase diagram denotes the liquidus, where solid ice forms co-exist with a fluid richer in ammonia.[24] The dotted line on the ADH phase diagram shows the dehydration boundary where solid ADH structures break down into a mixture of solid ice and AHH.[8,24] The dashed arrows show the P-T path taken to form the DMA phase in both compositions in Refs. 9, 10, and 24. The P-T path begins at room temperature where the samples are cooled until they solidify and are then compressed to a pressure of 5 GPa or above before being warmed to room temperature where the sample transforms to the DMA phase. For ADH, the sample must first be an amorphous solid formed by flash freezing the sample and can transform to the DMA phase at low temperatures upon compression, unlike AMH-DMA which only forms while being warmed to room temperature.

partially on single-crystal data—on the structure of AHH-II. And although they report a transition to DMA at 19 GPa, they observe two reflections in their diffraction data—one at 2.275 Å and the other at 2.15 Å—where only one reflection would be expected.[9]

In addition to the doubt over the structure of the crystalline phase produced on compression through the melting line at room temperature, it is unclear whether DMA is ever the phase with the lowest free energy. At room temperature, compression of all compositions richer in water than 2:1 ammonia:water—compositions richer in ammonia than 2:1 have not been studied—produces AHH-II and ice VII, and this configuration is stable—in the sense that it does not change with time on a timescale of weeks—up to at least 9 GPa.[9,10] In contrast, low-temperature compression and warming to room temperature above 6 GPa produces the DMA structure (in both 1:1 and 1:2 compositions) which also does not decompose with time on the same timescale. Further complicating this picture are the aforementioned observations of Ma *et al.* at 19 GPa and 25 GPa, and additionally the absence of diffraction studies above ambient temperature. In this paper, we report the results of synchrotron x-ray and neutron diffraction studies up to 530 K and 30 GPa which explore the relationships between AHH-II and DMA and assist in the resolution as to what the stable structures are in this complicated and planetary relevant system.

II. EXPERIMENTAL

The work described here has been performed using neutron diffraction techniques for deuterated samples in Paris-Edinburgh (P-E) presses[12] and complimentary x-ray diffraction studies using both hydrogenous and deuterated samples in diamond anvil cells (DACs) at the Diamond Light Source synchrotron. Neutrons offer the advantages of improved contrast between nitrogen and oxygen—whose x-ray cross sections are very similar—and the fact that the deuterium atoms contribute much more strongly to the neutron diffraction pattern than they do to the x-ray pattern. However, x-ray studies are able to explore the pressure and temperature range beyond that currently achievable by neutron diffraction in a P-E press.[13]

A. Sample preparation

The sample preparation technique has been described in detail elsewhere[8,14] and will only be described in brief here. A small mass of ammonia is condensed into an empty container at 80 K. A corresponding mass of water (to form the desired molar ratio of ammonia:water) is placed in a second vessel and cooled to liquid nitrogen temperatures. The ammonia is then condensed into the water-containing vessel to form the ammonia hydrate.

B. Neutron diffraction experiments

Neutron diffraction data were collected using the PEARL instrument at the ISIS pulsed-neutron source at the Rutherford-Appleton Laboratory in the UK. The PEARL instrument is dedicated to performing high-pressure experiments using the P-E press which allows large volume samples to be taken up to approximately 30 GPa.[13] To load the samples, an assembly composed of the anvils (made from tungsten carbide or sintered diamond), a clamping mechanism, and the TiZr (null scattering) encapsulated gasket[15] was cooled to liquid nitrogen temperatures. The ammonia hydrate solution (held at ~240 K) was poured into the sample chamber of the gasket. The assembly was put together and immersed in liquid nitrogen. The assembly was then transferred to a pre-cooled V4 P-E press (held at 170 K in a cryostat) and a sealing load of ~5 tonnes applied. The cryostat and press were placed on the PEARL instrument and data collected using the 90° detector bank. The data were corrected for the effects of anvil attenuation.[16] The corrected data were analysed by Rietveld profile refinement using the GSAS suite of programs.[17,18]

C. X-ray diffraction experiments

Synchrotron x-ray diffraction data were collected at the I15 Extreme Conditions beamline of the Diamond Light Source in DACs. Two types of DAC were used, Merrill-Bassett (M-B) cells[19] were used in heating experiments, and a Diacell Bragg-(S) DAC (Almax-Easylab) (DXR)[20] was used to explore the highest pressure ranges as this type of cell offers improved anvil alignment compared to that available for M-B cells. X-ray data were collected on a Mar345 image plate detector with an x-ray wavelength of 0.4254(1) Å determined by calibration with a silicon standard sample. All samples were loaded under the same conditions used for the P-E press experiments. The gaskets used for the compression experiments in the DXR cells were made of 200 μm thick tungsten, pre-indented to a thickness of ~50 μm with 125 μm diameter gasket holes. In the heating experiments, rhenium gaskets were used, as steel gaskets are known to react with ammonia and water samples at elevated temperatures,[6,21] and it was found that tungsten also reacted with the samples when heated. The rhenium gaskets prepared for the M-B cells were 270 μm thick, pre-indented to a thickness of ~30μm, and had 100 μm diameter gasket holes. In all x-ray samples, a small ruby sphere was included in the sample chamber for use as a pressure calibrant.[22] The x-ray beam was 50 μm in diameter and the diffractometer constants were determined by calibration with a silicon standard. The 2-D images were processed and integrated with the Fit2D software[23] before being exported for Rietveld refinement using the GSAS suite of programs.[17,18]

III. RESULTS AND DISCUSSION

In the work by Ma *et al.*,[11] a 2:1 ammonia:water solution first crystallises at room temperature on compression between 3.1 and 4.3 GPa as expected. At ~19.2 GPa, Ma *et al.* reported that the sample formed the AHH-DMA phase.[11] This pressure is much higher than the pressure of 5.5 GPa required to produce AMH-DMA and ADH-DMA, respectively, in samples with 1:1 and 1:2 composition when compressed at low temperature and then warmed to room temperature. In this work, we have attempted to form AHH-DMA at lower pressures; by following this low-T compression path, by decompressing AHH-DMA formed through compression at room temperature

and finally by heating a 2:1 sample at pressure. In the interests of presenting these results in the clearest way possible, the results have been grouped together by the initial as-prepared sample composition (ammonia:water ratio), and we describe the solid phases that are observed to form within each of these different sample compositions.

A. Compression study of deuterated 1:2 samples using neutron and x-ray diffraction

A 1:2 ammonia:water ratio solution was prepared and loaded using the neutron powder diffraction technique described in Sec. II using double toroidal anvils[13] allowing access to pressures in excess of 19.2 GPa required for the transition to AHH-DMA.[11] As described previously[8] by loading a 1:2 solution at room temperature and compressing, the sample solidifies into a mixture of AHH-II and ice VII, allowing the ice VII to be used as a pressure marker. Figure 3 shows the series of patterns collected on the deuterated 1:2 sample as load was increased. The sample first solidifies into a mixture of AHH-II and ice VII as is expected. Two features become clear from the patterns. Comparison of the observed d-spacings (including those of ice VII) with those observed by Ma *et al.*[11] reveals that the samples have similar diffraction patterns and that the orthorhombic AHH phase of Ma *et al.* is in fact a mixture of AHH-II[8] and ice VII. This of course implies that the sample of Ma *et al.* did not have exactly the 2:1 ammonia water ratio claimed but was in fact richer in water than this composition. It also is quite clear from Figure 3 that no transformation to the bcc AHH-DMA phase is observed for AHH-II up to the maximum pressure of 26.6 GPa, although it is possible that a transformation to the DMA phase has begun at this pressure, since, the relative intensities of the three most intense reflections of AHH-II ($(12\bar{1})$, (102), and (023)) have begun to change in this pattern. It is therefore clear, at least for deuterated samples, that the AHH-II to DMA transition occurs at a significantly higher pressure than previously reported, if at all.

To determine if the changing intensities observed in the last diffraction pattern in Figure 3 are the first sign of a transition from AHH-II to the AHH-DMA phase, a deuterated sample must be taken to pressures beyond those which are currently achievable in a P-E press. For this reason, a set of deuterated samples were studied on the I15 beamline at the Diamond Light Source in DACs, where pressures in excess of 30 GPa can be reached. The x-ray powder diffraction data collected from a deuterated 1:2 sample compressed at room temperature are shown on the right of Figure 4. The behaviour of this deuterated sample was very different from the deuterated 1:2 sample studied in the neutron powder diffraction experiment (summarised in Figure 3). In this x-ray experiment, ice VII forms first in the sample at 2.5(1) GPa as expected,[24] and after further compression to 7.6(1) GPa one singular peak forms at ~2.38 Å, consistent with the (110) bcc reflection for AHH-DMA. The reason for this unexpected behaviour of the 1:2 x-ray sample could be a result of the rapid compression from 2.5(1) to 7.6(1) GPa, compared to all the other samples studied, where the AHH-II phase was formed close to the crystallising pressure (3.5(1) GPa[8]). Another possible explanation for the difference could be the presence of ice VII in the sample, which has a crystal structure very similar to that of the DMA phase,[8] and could potentially act as a seed crystal to the DMA phase allowing it to form more readily; however, the presence of ice VII does not seem to have affected the 1:2 sample studied by neutron powder diffraction.

B. Compression study of a deuterated 1:1 sample using X-ray diffraction

Figure 4 also shows the x-ray powder diffraction data collected for a 1:1 deuterated ammonia:water sample (left

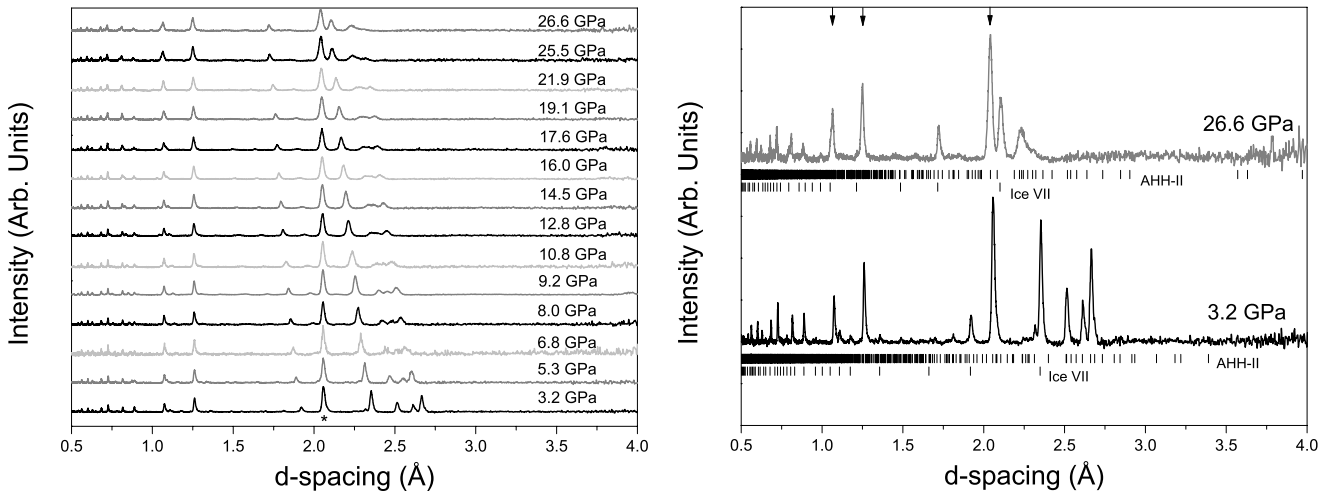

FIG. 3. Neutron powder diffraction data collected on a 1:2 deuterated ammonia:water sample. The asterisk (*) shows the most prominent reflection in the patterns caused by the sintered diamond anvils. The change in the relative intensities of the $(12\bar{1})$, (102), and (023) peaks in the sample between the lowest and the highest pressures appears to suggest that there is a phase transition in the very last pattern at 26.6(1) GPa, the emerging phase cannot be confirmed to be AHH-DMA because the transition is not complete and there is a large overlap with the $(12\bar{1})$, (102), and (023) reflections of AHH-II. The pressures shown in this figure were calculated from the equation of state of ice VII.[26] Since each powder pattern was collected over differing lengths of time, they have been rescaled so that the diamond peaks are of comparable size to one another. The first and last neutron powder diffraction patterns have been reproduced in the right hand figure for ease of comparison. The tick marks for the peaks associated with AHH-II and ice VII are shown for both plots.

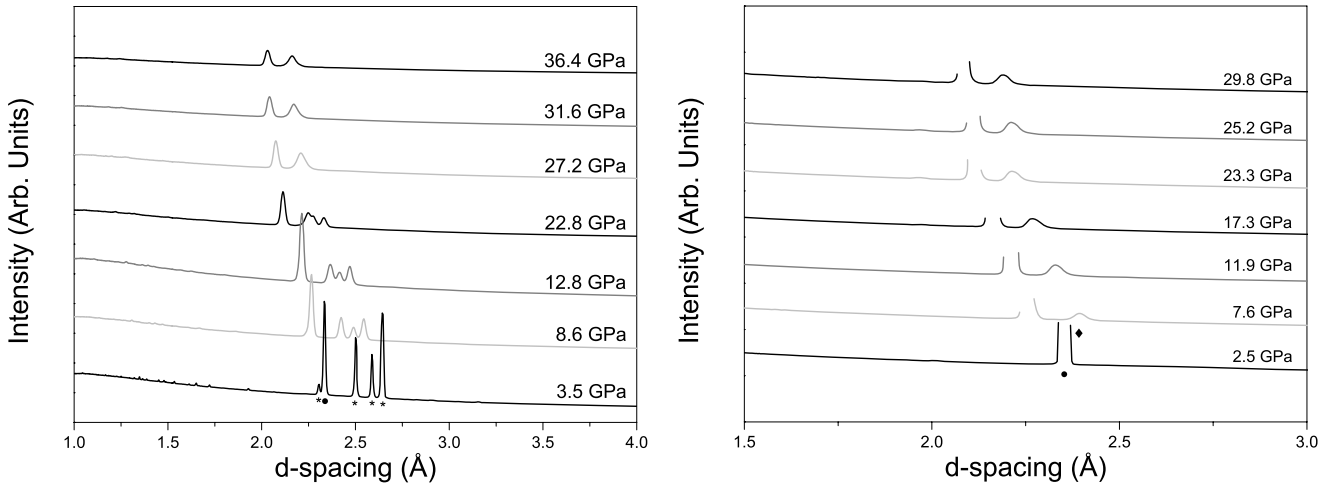

FIG. 4. X-ray powder diffraction patterns of a deuterated 1:1 ammonia:water sample (left) and a deuterated 1:2 sample (right). The pressures were measured using the ruby fluorescence method.[22] The behaviour and patterns in the 1:1 sample are very similar to that observed in the data presented in Figure 5. A structural transition is observed between 22.8(3) and 27.2(2) GPa where the three prominent AHH-II ($12\bar{1}$), (102), and (023) reflections are again replaced with a single AHH-DMA (110) reflection consistent with Figure 5. Note that the (110) reflection in the patterns associated with ice VII, marked with the filled circles (•) are several times larger than in the 2:1 sample in Figure 5. The 1:2 x-ray powder sample data show different behaviour from the neutron powder sample in Figure 3, forming AHH-DMA and ice VII without forming the AHH-II phase, see text for details. The asterisks (*) show the ($12\bar{1}$), (102), (023), and (040) reflections associated with the AHH-II phase, the full circle (•) shows the (110) reflection associated with ice VII. The diamond (♦) shows the AHH-DMA (110) reflection where it first forms in the 1:2 sample. Note that in the 1:2 sample data, the ice VII(110) reflection has been truncated for clarity.

hand figure). The 1:1 sample first solidifies as a mixture of AHH-II and ice VII at 3.5 GPa as expected[8] and again shows a marked resemblance to the x-ray patterns reported by Ma *et al.* with a much larger contribution from excess water ice, as would be expected. A transition to a phase that is consistent with the AHH-DMA structure can be seen at a pressure of 27.2(1) GPa, 8 GPa higher than that reported by Ma *et al.*;[11] however, this appears to be consistent with the 1:2 neutron powder diffraction experiment summarised in Figure 3 and described above where in a deuterated sample, the transition to the AHH-DMA phase was not observed up to a maximum pressure of 26.6 GPa.

C. High-pressure behaviour of 2:1 ammonia:water samples

This section describes the behaviour of two deuterated and one hydrogenous 2:1 ammonia:water samples. One deuterated sample was compressed in a DAC and subsequently decompressed and studied with x-ray powder diffraction, similar to the route used by Ma *et al.*[11] The other deuterated 2:1 sample was compressed at 170 K before subsequently being warmed to room temperature and studied with neutron powder diffraction, similar to the route used to form AMH-DMA and ADH-DMA.[9,10] The hydrogenous sample was heated at high-pressure and studied using x-ray powder diffraction to explore the potential of new methods for entering the AHH-DMA phase.

Figure 5 shows the x-ray powder diffraction data collected on compression of the 2:1 deuterated ammonia:water sample. Starting at a pressure of 3.8(2) GPa, the sample can be fitted with the AHH-II phase with a small excess of water present as ice VII, again as expected.[8] As was seen in the 1:1 deuterated sample (see above), beyond 26.5(2) GPa there is a change in the sample which is consistent with a phase transition to the AHH-DMA structure. The sample was compressed without further change to 41.0(5) GPa and no evidence was seen of the second transition reported by Ma *et al.*[11] From this maximum pressure of 41.0(5) GPa, the sample pressure was then decompressed in steps. As Figure 5 shows the DMA phase persisted down to the lowest measured pressure of 9.5(4) GPa, after which the sample was accidentally lowered to a pressure of 1.1(1) GPa and became liquid once more. However, starting at 19.2(1) GPa, a new feature can be observed at a d-spacing of ~2.37 Å (highlighted in Figure 5 with asterisks) along with the (110) bcc reflection of the DMA phase at ~2.27 Å (denoted by the filled circles in Figure 5). This new feature may be an evidence of the onset of the reverse DMA to AHH-II transition since it appears at the expected position of the ($12\bar{1}$) AHH-II reflection, but this cannot be confirmed from the data presented here. However, it is clear that there is hysteresis of at least 8 GPa in the pressure of the AHH-II to DMA transition, and there is evidence that this transition is very sluggish on decompression.

As has been stated in Sec. I, in both 1:1 and 1:2 ammonia:water compositions, the transition to a DMA phase is observed when the sample is compressed at ~170 K to ~60 tonnes of applied load—which corresponds to a generated sample pressure of 5-6 GPa—and then warmed to room temperature[9,10] (see Figure 2). A neutron diffraction experiment was conducted using very similar methods to those used in Refs. 9 and 10 on a 2:1 sample to establish if the same P-T path could be used to form the AHH-DMA phase.

Once the sample had been prepared and loaded into the P-E press as described in Sec. II, the applied load on the P-E press piston was increased in 10 tonnes steps up to a maximum of 55 tonnes at 170 K (the observed powder patterns are shown in Figure 6). The left hand figure of Figure 6 shows the neutron powder pattern of a 2:1 ammonia:water sample at 170 K and a sealing load of 5 tonnes along with a Rietveld refinement of

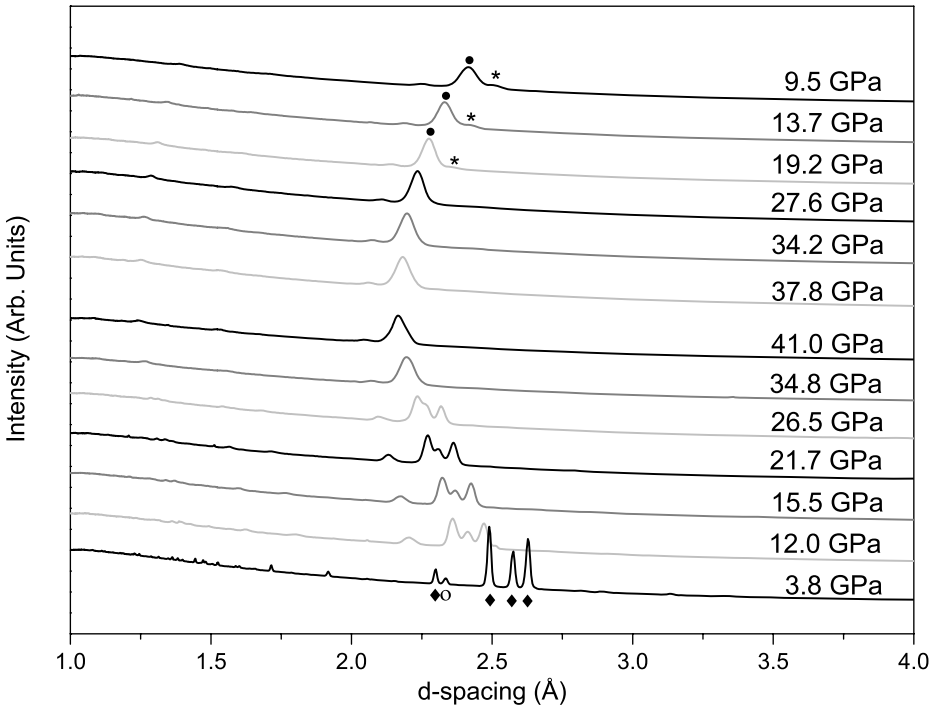

FIG. 5. X-ray powder patterns of a deuterated 2:1 ammonia:water sample as a function of pressure. The sample was compressed from 3.8(2) GPa to 41.0(5) GPa before being slowly decompressed to 9.5(4) GPa. The pressures were measured with the ruby fluorescence method.[22] The peaks highlighted with the filled diamonds (♦) belong to the AHH-II phase, the hollow circle (○) highlights an ice VII (110) reflection showing a slight excess of ice in the sample. The filled circles (●) show the peak associated with the AHH-DMA (110) reflection, and the asterisks (*) highlight the unidentified peak that emerges when decompressing at 19.2(1) GPa and below, which could identify transitioning back to AHH-II. A change in structure, where the three prominent AHH-II (12$\bar{1}$), (102), and (023) reflections are replaced with a single AHH-DMA (110) reflection, is observed to occur between 26.5(2) GPa and 34.8(1) GPa. Upon decompression, this phase remained stable to 9.5(4) GPa.

the pattern using the orthorhombic (Pbnm) AHH-I structure[14] and the difference curve between the observed and calculated intensities. The fit in this figure is to the AHH-I structure and accounts for the majority of the diffraction peaks observed in the pattern, the remainder can be accounted for by contributions from the sintered diamond anvils and a small amount of ammonia-I in the sample. The small contribution in the powder pattern from ammonia-I suggests that there was a slight excess of ammonia in the sample. Upon compression to 55 tonnes, the sample appears to go through 2 phase transitions, from AHH-I to an intermediate phase at a load of 15 tonnes, before entering a phase that shows several overlapping peaks at a d-spacing of approximately 2.6 Å shown in Figure 6.

Once at an applied load of 55 tonnes, the sample was slowly warmed to room temperature at constant applied load, during which no change in the powder pattern were observed, which can be seen in Figure 7. It is quite clear from Figure 6 that the pattern observed is not what is expected from a bcc structure. The expected reflection positions are shown by the tick marks of bcc AMH-DMA (the nearest comparable structure) in Figure 7.

Two other samples were also used in this experiment, but contained excess water. This was evident from the relative ammonia and water weights during the sample preparation process (these samples were calculated to have ammonia:water ratios of 1.94(1):1 and 1.92(2):1 compared to the third sam-

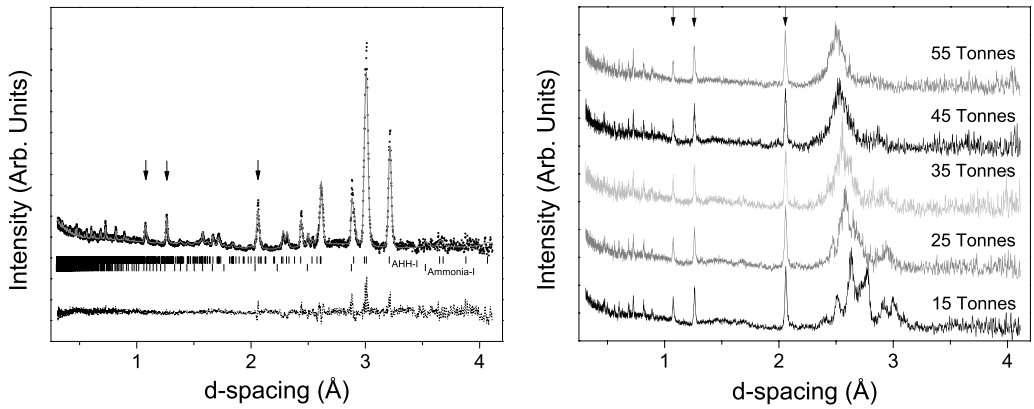

FIG. 6. The neutron powder diffraction data recorded on a 2:1 sample following the same P-T path used to produce both AMH-DMA and ADH-DMA, as described in the text. The left hand figure shows the result of the Rietveld refinement of the AHH sample at 170 K as loaded at the sealing load of 5 tonnes. The dots are the data points, the solid line shows the calculated pattern, and the dashed line below is the difference between the observed and calculated pattern. The arrows show the three most prominent peaks from the sintered diamond anvils. The upper tick marks show the peak positions from the AHH-I structure and the lower tick marks show the peak positions for the ammonia-I structure. The right hand figure shows the powder patterns observed upon slow compression of the sample to the applied load of 55 tonnes in 10 tonnes steps, equivalent to a change in pressure of (0.5-1 GPa). The arrows show the location of the three most prominent diffraction peaks in the pattern from the sintered diamond anvils. It is clear that there is a transition to an intermediate structure upon increasing the load to 15 tonnes, as seen by the change in the diffraction pattern from that shown in the left hand figure, and that the phase obtained at a load of 55 tonnes is not a cubic DMA phase.

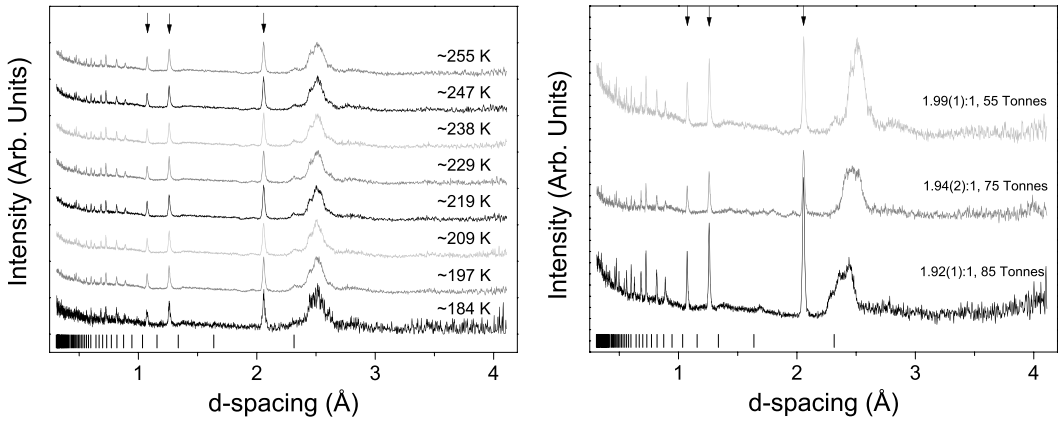

FIG. 7. The left hand figure shows neutron diffraction data collected on a sample loaded with an ammonia:water ratio closest to the ideal 2:1 ratio warmed to room temperature at an applied load of 55 tonnes. The arrows show the three most prominent peaks in the patterns caused by the sintered diamond anvils. The tick marks at the bottom of powder patterns show the expected positions of DMA phase peaks based on the structure of AMH VI. The right hand figure shows three different loadings of an AHH sample with different ammonia:water ratios that were warmed to room temperature at pressure. The top most powder pattern on the right hand figure corresponds to the top most plot of the left hand figure. Again the arrows show the three most prominent peaks in the patterns caused by the sintered diamond anvils and the tick marks show the expected peak positions of AMH VI at ~5 GPa (55 tonnes load).

ple's 1.99(1):1) and from the low-temperature powder patterns, which contained peaks identified as AMH-I as well as AHH-I. These samples were compressed to a maximum load of 75 and 85 tonnes, respectively, both at a temperature of 170 K before being gradually warmed back to room temperature at constant load. The patterns collected from the compressed samples once recovered to room temperature are shown in Figure 7, where the powder diffraction patterns of all three samples can easily be distinguished from one another, as the relative intensities of the most prominent sample peaks differ in each pattern and do not appear at the correct d-spacings to be accounted for by the bcc DMA structure.

We have also explored the high-temperature behaviour of the phase diagram using x-ray diffraction at the I15 station at the Diamond Light Source. A hydrogenous 2:1 ammonia:water ratio solution was loaded into a Merrill-Bassett DAC with a rhenium gasket using the process described in Sec. II. The cell was heated by a ring heater in thermal contact with the outside of the cell and the temperature was measured with a K-type thermocouple on the back of one of the diamond anvils. Once solidified (by compression at room temperature), the sample was heated. A hydrogenous sample with a 2:1 composition was explored over two heating cycles at two different initial pressures. The first heating cycle is shown in Figure 8 beginning at 4.0(1) GPa and 61(2) °C. In this pattern and those up to the pattern collected at 4.0(2) GPa and 80(3) °C, peaks of both AHH-II and bcc DMA (marked respectively with (*) and (•) symbols in Figure 8) are apparent. On compression and warming, to 87(2) °C and 4.7(1) GPa, the sample transformed completely to DMA. The sample was heated to 95(1) °C and although the (110) reflection disappeared, this appears to be the result of the reorientation of crystallites in the rather poorly averaged powder rather than melting because the (400) reflection remained visible. When the sample was compressed to 5.9(1) GPa at 95(3) °C, it showed evidence of transforming back to AHH-II and peaks of both AHH-II and DMA are visible. On warming and compression to 6.0(1) GPa and 105(1) °C, the transformation had reversed and only peaks from DMA are visible. On further compression and warming, the peaks from DMA disappeared between 6.6(1) GPa and 185(2) °C and 5.7(2) GPa and 214(4) °C leaving only a diffuse liquid halo. The sample was left to cool overnight and the second cycle of heating was started at 7.5(1) GPa and 20 °C (room temperature) where the sample showed only peaks from AHH-II (Figure 9). On warming the sample transformed to DMA between 7.0(1) GPa and 108(2) °C and 7.3(1) GPa and 118(2) °C. Further changes in temperature and pressure located melting of DMA between 6.2(1) GPa and 208(2) °C and 5.8(1) GPa and 209(2) °C, freezing of liquid to DMA between 6.5(1) and 7.4(2) at 209(3) °C and melting of DMA between 6.4(2) GPa and 257(5) °C and 6.6(2) GPa and 252(5) °C. Additionally, the lattice parameter for the AHH-DMA phase at 4.8 GPa and 89 °C is a = 3.578(2) Å calculated from the d-spacing of the (110) reflection. This is the most comparable pressure and temperature to that reported for AMH-DMA and ADH-DMA (5.5 GPa and room temperature[9,10]) and is again comparable in magnitude, although larger than both as a result of the lower pressure and higher temperature. Taken together with the lattice parameter calculated for 9.5(4) GPa of a = 3.296(4) Å, this would suggest that AHH-DMA has a lattice parameter ~3% larger than those of both AMH-DMA and ADH-DMA whose lattice parameters appear not to depend strongly on composition[9,10] at the same pressure and temperature.

D. Discussion

As we have seen, our results are consistent with the result of Ma *et al.*[11] below 25 GPa once it is recognised that the sample of Ma *et al.* contained more water than the claimed 2:1 ammonia:water ratio and hence contains ice. Our studies confirm an AHH-II to DMA transformation at high pressure and room temperature and reveal an 8 GPa increase in the upstroke transition pressure on deuteration. This is a large isotope substitution effect. We find no evidence for the second transition reported by Ma *et al.* at 25 GPa[11] in an hydrogenous sample since we find that DMA persists unchanged up to 41.0(5) GPa in a deuterated sample. This difference could of course be an even larger (15 GPa) deuteration effect but we

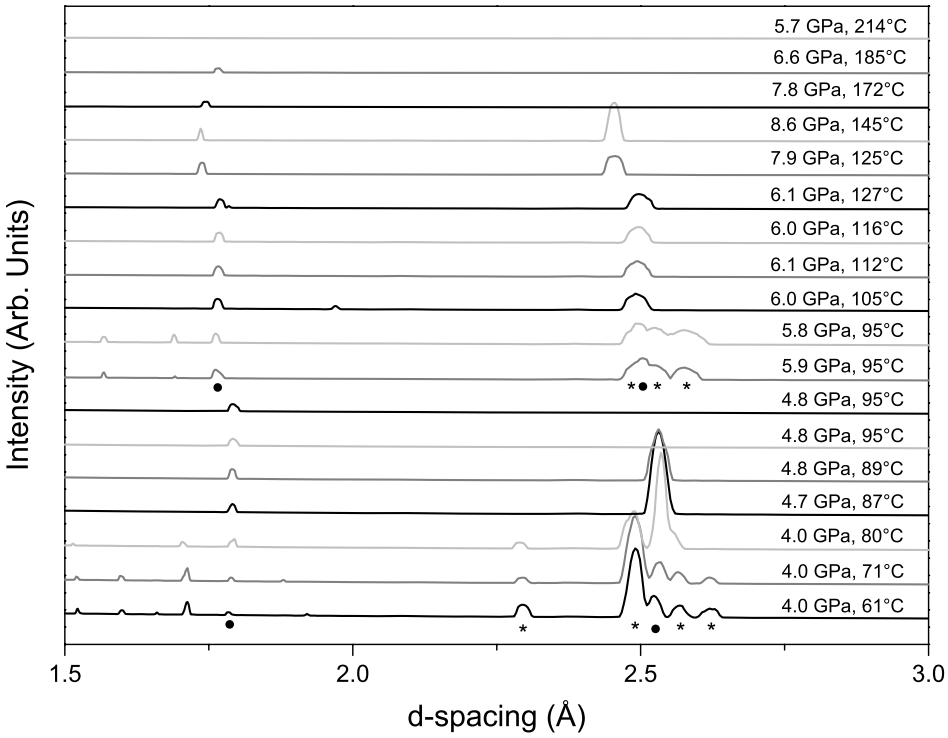

FIG. 8. X-ray powder diffraction data of a hydrogenous 2:1 ammonia:water sample as it was heated over its first heating cycle from 4.0(2) GPa at 61(2)°C to 5.7(2) GPa at 214(4)°C. The pressures were measured with the ruby fluorescence method and temperatures measured from the back of the diamond anvils. Several transitions from the AHH-II phase to the bcc DMA phase are observed along with a transition from the DMA phase to the liquid phase which is preceded by the disappearance of the most intense diffraction peak and a broad "halo" of a liquid pattern observable in the diffraction image once through the transition, this is not observable in the 1D diffraction patterns as the feature is very broad and has much less intensity than the crystallographic reflections. Asterisks (*) show the peaks associated with AHH-II, filled circles (•) show those associated with AHH-DMA. The poor peak shapes are attributed to the highly textured nature of the sample.

argue that it is not the case. We note that the evidence for this transition in the data of Ma *et al.* comes from the diffraction data and there is no evidence for the transition in the Raman data.[11] Furthermore, in the data of Ma *et al.*, the transition is signalled by strong changes in the intensity of a peak at ~2.1 Å—this peak is in fact a reflection from ice VII that appears to become overlapped with a new emerging reflection—and the appearance of a second new peak at ~1.9 Å. These

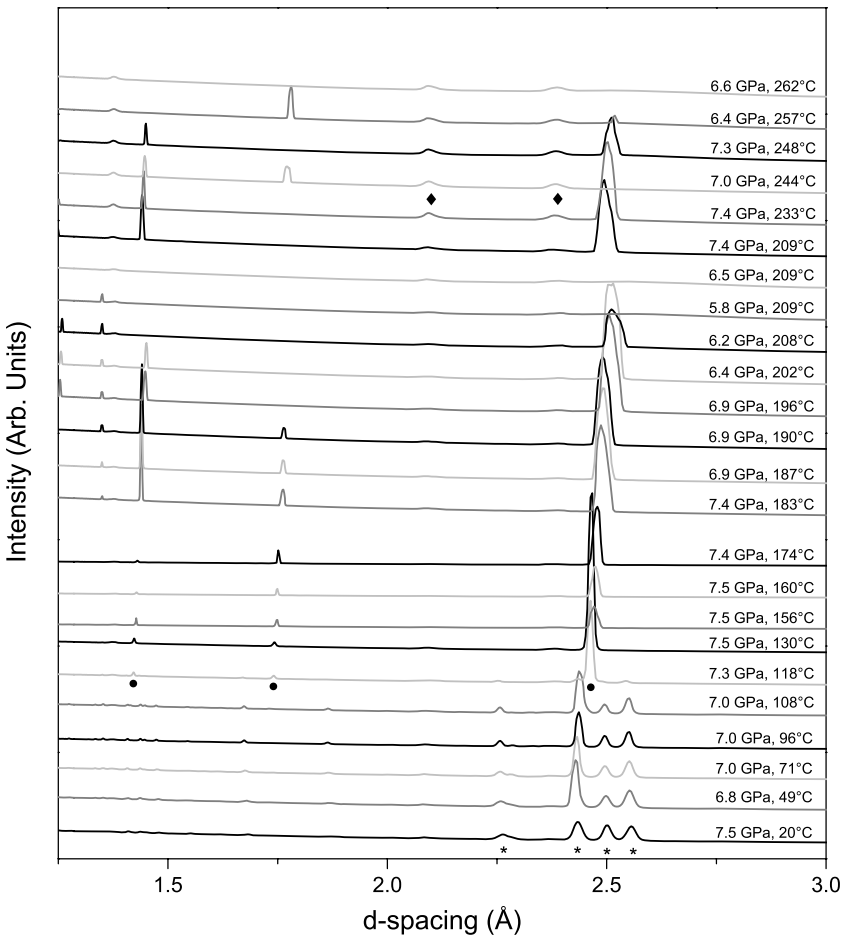

FIG. 9. X-ray powder diffraction data of a hydrogenous 2:1 ammonia:water sample as it was heated over its second heating cycle. Reflections associated with AHH-II are shown with asterisks (*), those associated with AHH-DMA are highlighted with filled circles (•), and diffraction peaks that belong to the rhenium gaskets are highlighted with filled diamonds (♦). Along with a clear transition to a bcc phase at 7.3(1) GPa at 118(2)°C, this phase can also be observed melting, at 6.5(1) GPa and 209(2)°C, and re-entering the bcc phase from the melt at 7.4(2) GPa and 209(2)°C. The irregular peak profiles are caused by the highly textured appearance of the sample.

new peaks have essentially pressure independent positions above 25 GPa. It thus may be that they are either peaks from the gasket material or the product of a reaction between that sample and the gasket, further studies are needed to confirm this hypothesis.

From the cold compression experiments, it appears that AHH-DMA does not form by following the same path used to form both AMH-DMA and ADH-DMA. From the collected neutron powder data, a new intermediate phase has been observed in a 2:1 ammonia:water ratio sample, this is the bottom pattern on the right hand side of Figure 6 at a load of 15 tonnes and a temperature of 170 K. The exact nature of this complicated pattern (mixed phase, decomposition of sample, new structural phase, etc.) has not been determined in this work, but the pattern is clearly distinct from the AHH-I pattern shown in the left hand figure of Figure 6. Additionally, as three separate loadings with minor differences in their ammonia:water ratios (1.92(2):1, 1.94(1):1, and 1.99(1):1) were all recovered to room temperature, but exhibited differing powder patterns, this appears to suggest that the recovered samples are a mixed phase (the end products of these three samples are shown in the right hand figure of Figure 7).

These results of the heating experiment are summarised in Figure 10 along with tentative phase boundaries for the liquid to AHH-DMA and AHH-DMA to AHH-II transitions. The fact that both of these boundaries can be crossed reversibly provides the first direct evidence that (at least for the 2:1 ammonia:water composition) DMA is a thermodynamically stable phase and not a metastable form with frozen in disorder. Previously, most of the observations of DMA had been made in samples compressed at low temperature and warmed and hence the question of metastability was open. This has important potential consequences for planetary modelling since in any planet or satellite where the P-T profile crosses the AHH melting line above ~4 GPa (the lowest pressure at which we observed DMA), the solid phase formed will be DMA and not AHH-II. This has effects for the modelling of the heat produced by freezing, since DMA will have a lower latent heat of fusion than AHH-II because it has a higher entropy. The fact that DMA forms directly from the melt may also have consequences for chemical differentiation in planetary bodies whose ammonia:water mixtures are generally richer in water than 2:1. We have now shown that the DMA structure exists for 2:1, 1:1, and 1:2 ammonia:water compositions. It thus is possible that, above 4 GPa, compositions richer in water than 2:1 form a DMA whose composition is the same as the liquid from which they form; that is, that DMA forms without precipitating ice VII. Below this pressure, our earlier work shows that liquids richer in water than 2:1 freeze to form AHH-II and ice VII. This possibility needs to be explored experimentally.

The conclusion that DMA is thermodynamically stable implies that the AHH-II to DMA transition is an order-disorder transition. As we have shown,[8] the molecular packings of AHH-II and DMA are very similar. The two phases differ in that AHH-II has long-range order of both the molecular orientations and of the species occupying each molecular site and at the transition to DMA these long-range features are lost. Thus, AHH-II provides a basis for a local snapshot of the disordered arrangement which fluctuates spatially and with time to give an average which is the DMA structure in a similar way to the way that ordered ice VIII provides basis for models of the local structure of disordered ice VII.[25] It should be noted that in our earlier work we found evidence for a low (10%) level of substitutional disorder in AHH-II.[8] This provides evidence to support the view that energy cost of disordering the AHH-II structure is low.

From the mixed AHH-II/DMA diffraction patterns, it is possible to estimate the volume difference between AHH-II and DMA. The values vary somewhat, but are always positive and lie in the range 1%-3%. The positive volume change is consistent with the observed increase in the critical temperature for the AHH-II to DMA transition and combined with a Clapeyron slope of 0.14 $GPaK^{-1}$ give a ΔS for the AHH-II to DMA transition of between 50-150 $JK^{-1}mol^{-1}$. If this entropy change is attributed entirely to configurational disorder, it corresponds to between 7.5 and 413 configurations for each molecular site in the DMA structure. The lower value

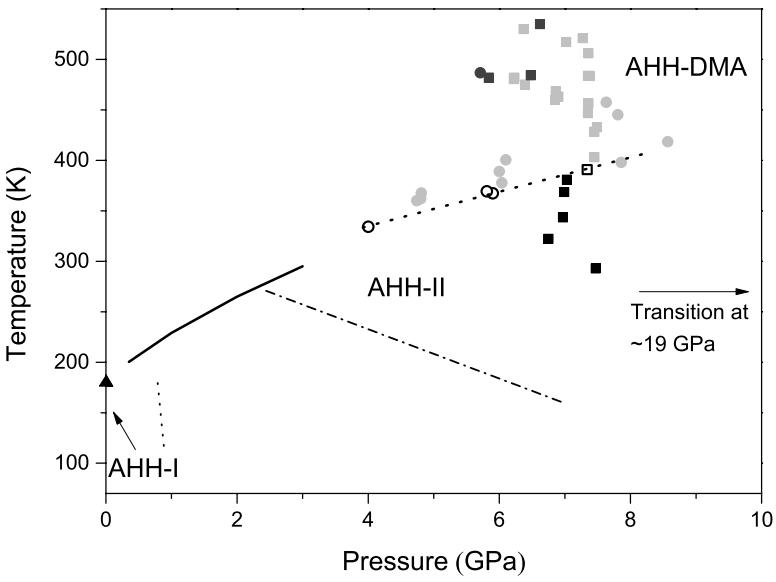

FIG. 10. Proposed phase diagram for hydrogenous AHH based upon the data collected in the heating experiment presented in Figures 8 and 9. The black symbols denote the P and T's where AHH-II was observed, the light grey where AHH-DMA phase was seen, and the dark grey show where the sample was fully molten. The open symbols show the P and T at which both AHH-II and AHH-DMA were observed. The different shapes show which points are from the patterns shown in Figure 8 (circle •) and Figure 9 (square ■). The open symbols show patterns that contained contributions from both AHH-II and the AHH-DMA phases. The dashed-dotted line shows the approximate area of the dehydration line where water rich samples break down into AHH-II and ice VII/VIII (see Figure 2) where AHH-II has yet to be observed experimentally. The dotted line shows the phase boundary estimated from the pressure at which the 2:1 neutron sample started to transform (see Figure 6). The triangle (▲) is where deuterated AHH is observed to freeze in the solid AHH-I phase at ambient pressure[14] and the solid line shows the melting curve of AMH as determined by Hogenboom *et al.*[27]

is plausible for a disordered structure given that in addition to the N/O substitutional disorder, there is also orientational disorder of the molecules. The higher value seems too large to be plausible, hence, it appears that the volume difference between AHH-II and DMA is closer to 1% than 3%. Clearly, more accurate measurements of this quantity are needed. The fact that a transition between AHH-II and DMA is observed at room temperature at much higher pressures (25-30 GPa) implies that the transition temperature must have a maximum somewhere between 7.5 GPa and 25 GPa and further work is required to locate the maximum. Finally, although we observed melting in our samples, the data do not provide sufficient information to extend the melting line. There is thus a clear need to make measurements of the melting lines of all three compositions of ammonia hydrates in the pressure range above 3 GPa.

Finally, it is worth noting the 3% difference in lattice parameters between DMA with compositions of 2:1 and 1:1 and 1:2. At ambient pressure, the volume per-molecule of ammonia hydrates is almost composition-independent.[8] The fact that at 6 GPa we estimate the volume per molecule to be 9% larger in 2:1 DMA than the other two compositions suggests some profound difference which would benefit further investigation.

IV. CONCLUSIONS

As we have seen, our results provide the first evidence of transitions from the AHH-II phase to and from the DMA structure, as well as direct transformation from the DMA phase to the liquid phase. They thus provide the first evidence that this unique structure is indeed a thermodynamically stable phase. They also provide new information on the boundaries and transition behaviour of the 2:1 ammonia:water composition. We have been unable to produce the DMA structure in this composition by the low temperature compression and warming route that produces DMA in the 1:1 and 1:2 compositions. We have also confirmed the direct compression transformation from AHH-II to DMA observed by Ma *et al.*[11] and shown that this transition has a large (8 GPa) deuteration effect.

ACKNOWLEDGMENTS

The authors would like to thank both the EPSRC and STFC for both funding and provision of beam time at both the Diamond Light Source and the ISIS Pulsed-Neutron Source. Thanks also to the I15 team (Heribert Wilhelm, Annette Kleppe, Dominic Daisenberger, and Allan Ross) for their help in collecting the x-ray data and providing their scientific and technical support while on experiment. Thanks also to Andy Chamberlin and Chris Goodway from ISIS for their technical support on our neutron experiments.

[1]R. Helled, J. D. Anderson, M. Podolak, and G. Schubert, Astrophys. J. **726**, 15 (2011).
[2]G. Tobie, O. Grasset, J. I. Lunine, A. Mocquet, and C. Sotin, Icarus **175**, 496 (2005).
[3]J. S. Loveday and R. J. Nelmes, High Pressure Res. **23**, 41 (2003).
[4]T. Guillot, Annu. Rev. Earth Planet. Sci. **33**, 493 (2005).
[5]G. A. Jeffrey, *An Introduction to Hydrogen Bonding* (Oxford University Press, 1997), Chap. 10.
[6]H. C. Cynn, S. Boone, A. Koumvakalis, M. Nicol, and D. J. Stevenson, in *Proceedings of the 19th Lunar and Planetary Science Conference* (Cambridge University Press/Lunar and Planetary Institute, 1989), Vol. 1, p. 433.
[7]J. I. Lunine and D. J. Stevenson, Icarus **70**, 61 (1987).
[8]C. W. Wilson, C. L. Bull, G. Stinton, and J. S. Loveday, J. Chem. Phys. **136**, 094506 (2012).
[9]J. S. Loveday and R. J. Nelmes, Phys. Rev. Lett. **83**, 4329 (1999).
[10]J. S. Loveday, R. J. Nelmes, C. L. Bull, H. E. Maynard-Casely, and M. Guthrie, High Pressure Res. **29**, 396 (2009).
[11]C. Ma, F. Li, Q. Zhou, F. Huang, J. Wang, M. Zhang, Z. Wang, and Q. Cui, RSC Adv. **2**, 4920 (2012).
[12]J. M. Besson, R. J. Nelmes, G. Hamel, J. S. Loveday, G. Weill, and S. Hull, Physica B **181**, 907 (1992).
[13]S. Klotz, J. M. Besson, G. Hamel, R. J. Nelmes, and J. S. Loveday, Appl. Phys. Lett. **66**, 1735 (1995).
[14]J. S. Loveday and R. J. Nelmes, High Pressure Res. **24**, 45 (2004).
[15]W. Marshall and D. Francis, J. Appl. Crystallogr. **35**, 122 (2002).
[16]R. M. Wilson, J. S. Loveday, R. J. Nelmes, S. Klotz, and W. G. Marshall, Nucl. Instrum. Methods Phys. Res., Sect. A **354**, 145 (1995).
[17]A. C. Larson and R. B. Von Dreele, Los Alamos National Laboratory Report No. 86, 2004.
[18]B. H. Toby, J. Appl. Crystallogr. **34**, 210 (2001).
[19]L. Merrill and W. A. Bassett, Rev. Sci. Instrum. **45**, 290 (1974).
[20]Almax-Easylab, Diacell bragg-(s) product page, 2014.
[21]S. Boone and M. F. Nicol, in *Proceedings of the Lunar and Planetary Science Conference* (Lunar and Planetary Institute, 1991), Vol. 21, p. 603.
[22]R. A. Forman, G. J. Piermarini, J. D. Barnett, and S. Block, Science **176**, 284 (1972).
[23]A. P. Hammersley, "FIT2D: An introduction and overview," Tech. Rep., ESRF Internal Report No. ESRF97HA02T, 1997.
[24]A. D. Fortes, I. G. Wood, M. Alfredsson, L. Vočadlo, K. S. Knight, W. G. Marshall, M. G. Tucker, and F. Fernandez-Alonso, High Pressure Res. **27**, 201 (2007).
[25]R. Nelmes, J. Loveday, W. Marshall, G. Hamel, J. M. Besson, and S. Klotz, Phys. Rev. Lett. **81**, 2719 (1998).
[26]R. J. Hemley, A. P. Jephcoat, H. K. Mao, C. S. Zha, L. W. Finger, and D. E. Cox, Nature **330**, 737 (1987).
[27]D. Hogenboom, Icarus **128**, 171 (1997).